Sustainable Energy & Fuels

ROYAL SOCIETY OF CHEMISTRY

COMMUNICATION

View Article Online
View Journal | View Issue

Cite this: *Sustainable Energy Fuels*, 2020, **4**, 2661

Received 17th February 2020
Accepted 27th March 2020

DOI: 10.1039/d0se00263a

rsc.li/sustainable-energy

Polymer reinforced carbon fiber interfaces for high energy density structural lithium-ion batteries†

Kathleen Moyer,[a] Nora Ait Boucherbil,[b] Murtaza Zohair,[a] Janna Eaves-Rathert[b] and Cary L. Pint *[c]

Here, we show that for battery active materials coated onto carbon fiber current collectors, a thin electroconductive poly acrylonitrile, or PAN, coating applied to the surface of the battery material coated fiber drastically improves adhesion and multifunctional structural energy storage performance. With this electrode design, we demonstrate structural battery composites composed of lithium iron phosphate cathodes and graphite anodes which exhibit a maximum energy density of 58 W h kg^{-1} considering all combined battery and composite materials that make up both the energy storage unit and structural system framework it powers. These full-cell structural batteries also demonstrate capacity retention over 80% exceeding 100 cycles with an average energy density of 52 W h kg^{-1}. Combined mechanical and electrochemical testing correlates this excellent multifunctional performance to the role of PAN coating that adheres active battery materials to carbon fibers during battery operation and mechanical loading. Our findings demonstrate a structural Li-ion battery with a gravimetric multifunctional advantage for electrically powered systems, and highlights the importance of interface engineering to enable practical structural battery systems.

Introduction

While lithium batteries have been an enabling device for mobile applications, the basic method for incorporating the lithium-ion battery (LIB) into systems has remained unchanged over the past thirty years.[1,2] Traditional LIB architectures, including pouch, cylindrical, and prismatic cells, have remained independent of the system they power and involve materials and electrolytes packaged into self-contained cells, which are then added externally to a system that requires power input. Despite great strides since the conception of the lithium-ion battery to reduce inactive mass,[3] minimize packaging,[4,5] and streamline manufacturing,[6,7] performance improvements in batteries have been historically slow. While improved anodes give promise to higher cell capacity,[8–11] the push to reduce or eliminate cobalt from cathodes as battery production volume scales higher means lower cell voltage,[12,13] and this brings a push–pull competition toward improved battery performance at the cell level. In this regard, a growing number of current and emerging applications for LIBs depend on the system performance. For example, in electric vehicles the total mass footprint of the chassis, batteries, and other components is correlated to the power/energy requirements of the battery – *i.e.* a lighter EV chassis with the same battery pack is synonymous with the same EV chassis weight with a higher energy density battery pack. Despite this tradeoff for many systems ranging from drones, UAVs, electric vehicles, electric powered maritime vehicles, power tools/appliances, and more – researchers most commonly continue down this path to improve energy density through new electrode materials rather than better system integration methods.

With this said, structural energy storage represents a growing field of research over the past years. Early studies in this area primarily focused on supercapacitors with a simple two symmetric electrode design, and inspiration built from work on polymer and/or solid battery architectures.[14–21] Challenges among these early studies included a lack of clear justification for multifunctional operation and/or performance, and extremely low areal and gravimetric energy storage capability in the order of a few to tens of mF cm^{-1}.[2] While many of these challenges remain, efforts to benchmark multifunctional performance are starting to emerge. Sun *et al.*[22] highlight a comparison of improved rGO/Kevlar supercapacitors compared to carbon aerogel/epoxy materials and introduce a formalism to evaluate the multifunctional advantage in

[a]*Interdisciplinary Materials Science Program, Vanderbilt University, Nashville, TN 37235, USA*

[b]*Department of Mechanical Engineering, Vanderbilt University, Nashville, TN 37235, USA*

[c]*Department of Mechanical Engineering, Iowa State University, Ames, IA 50011, USA. E-mail: carypint@iastate.edu*

† Electronic supplementary information (ESI) available: Supporting information is available and contains galvanostatic half-cell testing for GR|Li and LFP|Li, coulombic efficiency data, rate performance of coated and uncoated devices, and calculations of multifunctional advantage. See DOI: 10.1039/d0se00263a

structural energy storage. While transitioning from supercapacitors to batteries opens the door to many orders of magnitude greater energy storage in a structural material, this path also brings more advanced challenges due to the electrode volume change associated with charging and discharging.[23] This requires advanced design criteria for structural batteries that can overcome stresses localized to interfaces, which are often a challenge to address in commercial batteries that are packaged under compression. This is likely the reason why early studies in structural batteries simply encapsulated packaged lithium-ion battery pouch cells into the composite layup process.[24–27] However, it is notable that this approach results in no gravimetric advantage for the system compared to simply just externally connecting the battery, and can result in a mechanical disadvantage for the composite at the battery packaging/epoxy interface. With this said, only recently have approaches been demonstrated for direct integration of battery materials into structural composites, but these approaches so far have demonstrated negligibly low energy density relative to the total mass of combined active and composite materials with moderate cycling stability[28–37] or moderate energy density and low cycling stability.[38]

Outside of structural batteries, it is known that surfaces and interfaces are critical to achieve stable, high performance energy storage.[39] One route toward the stabilization of battery material interfaces is by the use of ultrathin coatings applied by atomic layer deposition (ALD),[40–44] or polymer film reinforced battery electrode interfaces.[45–49] Shen *et al.*[50] show that vapor phase polymer coatings onto silicon anodes stabilize them against the extremely high volume change of silicon in lithium batteries. Along the theme of structural batteries and supercapacitors, recent studies have also made significant progress designing electrode architectures that can be drop-in components to multifunctional or structural battery design and sustain mechanical stress independent of interface coupling challenges.[51–55] With this said, with a growing broad research interest in studying structural supercapacitors and batteries that require stable energy storage operation under mechanical loading, there surprisingly have been little to no studies studying interfaces and interface design in these systems.

In this study we bring together these ideas to demonstrate the importance of interface engineering for multifunctional structural energy storage devices. Our work utilizes a thin PAN coating that "locks-in" the interface between the active battery material and the structural carbon fiber backbone of the composite material. We demonstrate this to drastically improve the performance of structural battery composites, yielding substantial improvements in energy density and stability compared to composites without PAN reinforced interfaces. Specifically, we demonstrate a gravimetric energy density of up to 58 W h kg^{-1} relative to combined active and inactive composite materials as well as cycling performance up to 100 cycles while maintaining > 80% capacity. This approach overall yields the first demonstrated structural battery that is advantageous to a system – *e.g.* the benefit to the performance of the system with the multifunctional battery is improved compared to a system with a separate battery and structural material combined.

Results & discussion

PAN is already commonly utilized for coating the surface of carbon fibers to enhance mechanical strength in lightweight carbon fiber composites. In this case, to utilize PAN as an interface engineering platform for structural batteries, we simply sandwiched the active battery material between the current-carrying carbon fiber materials and the PAN coating (Fig. 1a and S12, ESI†). In this design, the carbon fiber network doubles as the current collector and structural backbone of the device, while the PAN coating mechanically reinforces the carbon fiber-battery material interface and provides an electroactive transport medium for lithium ions. By using carbon fiber as a conductive and structural current collector backbone of the device, which displaces Al and Cu metals, a reduction of up to 15% of the gravimetric footprint of Li-ion batteries is achieved, which is advantageous for offsetting the mass penalty of incorporating battery systems in composites.[49] While some past work has considered carbon fiber as an electrode itself, lower capacity and the electrochemical cycling reversibility of Li[35–37] combined with structural degradation to the composite backbone during successive charge/discharge cycles make graphite coated onto a carbon fiber electrode a more practical selection for a high performance and stable structural battery design. This design incorporating graphite anodes and lithium iron phosphate cathodes (GR|LFP) is shown in Fig. 1b and contrasted to an electrode architecture without PAN coating. Notably, as PAN is commonly utilized for coating the surface of carbon fibers to enhance mechanical strength in lightweight carbon fiber composites, the case of our design with a PAN interface simply sandwiches the active battery material between the carbon fiber and PAN coating. Overall, when the carbon fiber current collector is subjected to either a concentrated mechanical force due to bending and/or interfacial shear stress due to successive charge–discharge cycles, our findings in this work indicate significant delamination of the battery active materials from the current collector that renders a portion of the material inactive for energy storage (Fig. 1b and S14, ESI†). In this regard, the PAN coating plays a (mechanical) role parallel to compressive packaging in commercial LIBs, which is to adhere the active battery material to the current collector to mitigate this problem. To demonstrate this point, Fig. 1c shows galvanostatic charge–discharge curves from structural LIBs prepared identically except with and without a PAN reinforcing interface following 100 cycles of galvanostatic charge–discharge cycling at a rate of 0.1 C. The lithium storage capacity normalized against all active and inactive materials in the structural battery is ~50% lower for the battery that is prepared without the PAN reinforcing interface due to delamination and loss of active materials.

Therefore, PAN addition results in better stability of the critical battery-structural material interface that minimizes material delamination. To further evaluate and demonstrate this, lap-shear tests were performed for both GR and LFP electrodes with and without PAN (Fig. 2a and b). The addition of PAN to the GR electrode increased the ultimate tensile strength

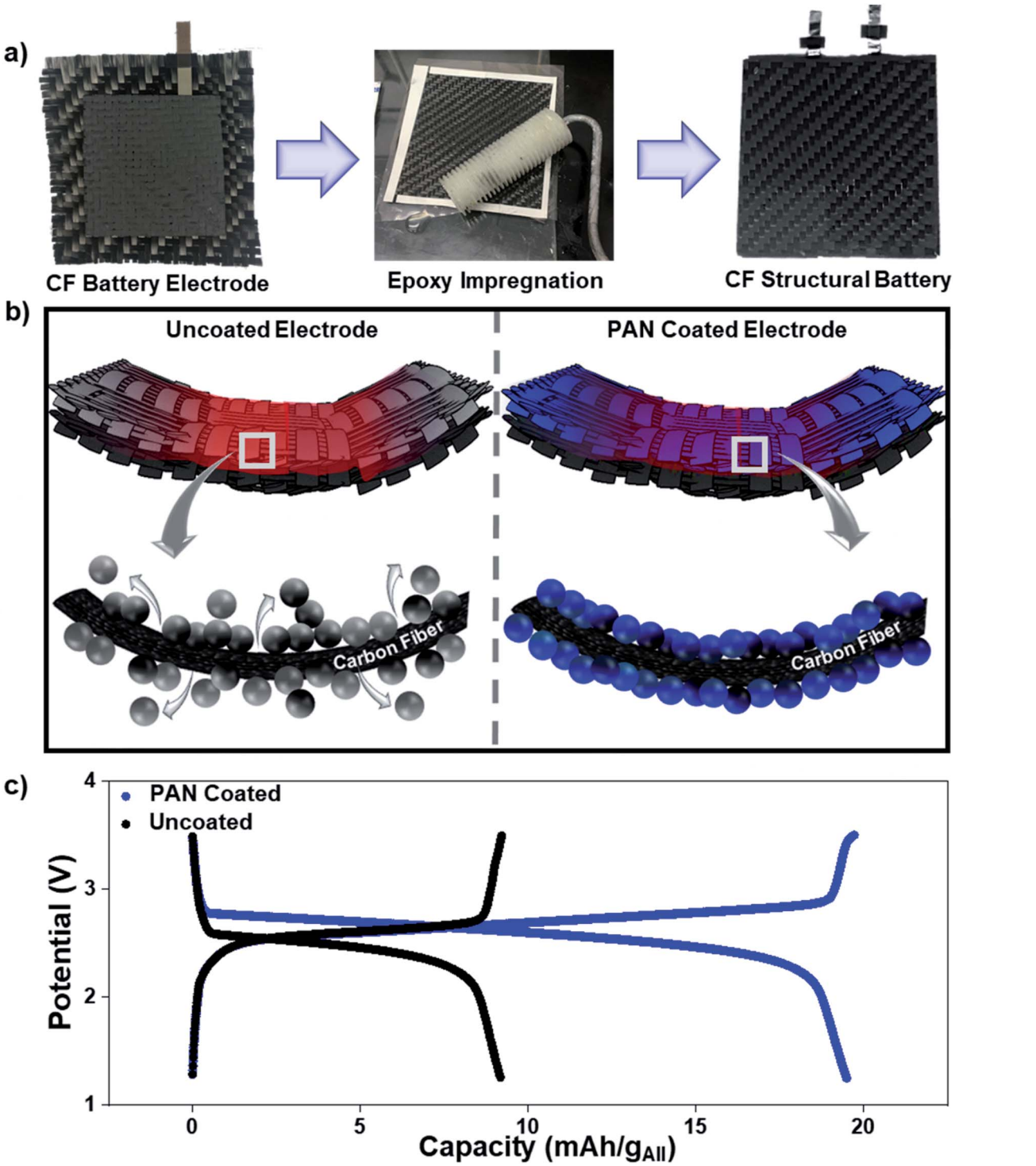

Fig. 1 (a) Fabrication of structural LIBs from battery electrodes to epoxy impregnation into structural composites, (b) scheme illustrating stress distribution and material delamination in carbon fiber structural battery electrodes with and without a PAN coating and (c) 100th galvanostatic charge discharge cycle at 0.1 C for uncoated (black) and PAN coated (blue) carbon fiber GR|LFP full-cells.

by >40% and that of the LFP electrode by >80%. As this test is designed to identify and test the integrity across interfaces, these results support that the PAN coating significantly augments the interfacial mechanical adhesion in the structural composite. As the carbon fiber – composite interfacial structure is critically important for structural composites, the fiber-matrix interphase requires chemical or mechanical linkage for the best performance.[56] In the case of a structural battery, the active battery materials coated onto the carbon fiber current collector directly make up this interphase region and, in turn, determine

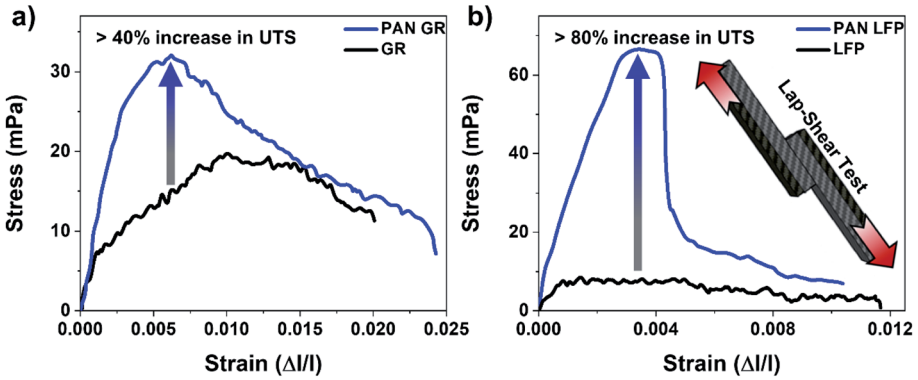

Fig. 2 Lap shear tests at rate of 2 mm min^{-1} for (a) GR and (b) LFP electrodes with and without PAN, and the inset showing the lap-shear test scheme.

the mechanical properties of the composite. Failure occurs at the weakest point in this matrix, which will always be at this interphase region due to the lack of chemical or mechanical binding of the active materials to the carbon fiber. Additionally, charging and discharging the battery materials on a static current collector imposes additional interfacial shear stress at the battery material/CNT interface to amplify this interfacial instability. In this way, the significantly improved mechanical properties in lap-shear tests of electrodes with PAN coating emphasize a more compact and adherent fiber-matrix interphase that reduces or eliminates interfacial delamination between the composite matrix and carbon fiber during battery operation and/or mechanical loading.

In addition to the mechanical properties, we performed further tests to evaluate the impact of the PAN layer on the electrochemical properties of the electrodes. Cyclic voltammograms (CVs) were obtained at 5 mV s^{-1} for both PAN GR|LFP (Fig. 3a) and GR|LFP electrodes (Fig. 3b). In the case of the PAN GR|LFP electrode, the faradaic redox couple appears to be stable over successive CV sweeps, which is in contrast to the GR|LFP electrode where the redox peaks evidently decrease in intensity and also shift to lower potentials during five successive CV scans. For the case without PAN, the reduction peak beyond the 1^{st} cycle for the GR|LFP electrodes is less pronounced which indicates that the Li-ions cannot as easily access the host LFP structure. Consequently, this CV appears more capacitive in nature and less reversible as there are fewer available sites for charge to be stored within the LFP cathode due to material delamination over the course of cycling. Material delamination is further evident by the magnitude of the peak current reduction for each electrode.[57] Between the 1^{st} and 5^{th} cycles, the peak current decreases by only ~5% for the PAN GR|LFP electrode but >75% for the GR|LFP electrodes. This reduction in peak current is associated with a decrease in the number of electrons associated with redox processes over the subsequent cycles, which is often attributed to a decrease in the electroactive surface area. As the surface area decreases and fewer electrons are needed to accommodate the redox activity of active electrode materials, this further supports the mechanism of delamination at interfaces for the instability of the electrode without PAN coating.

Further electrochemical testing of full-cell structural LIBs further supports the mechanism of PAN coating to improve interfacial adhesion and stability (Fig. 4). When PAN is coated onto the CF/battery electrodes (Fig. 4a), the initial capacity is greater than that without PAN (Fig. 4b). We attribute this to irreversible capacity loss due to delamination during formation cycling, where stresses during stable SEI formation on the

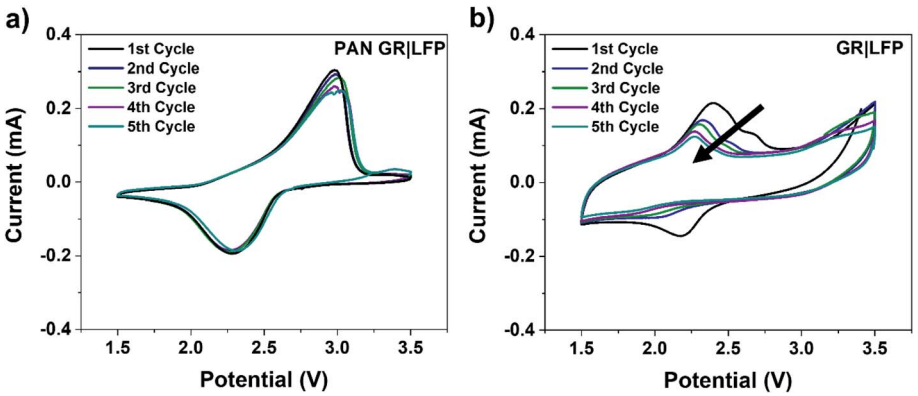

Fig. 3 Cyclic voltammograms at scan rate of 1 mV s^{-1} for (a) PAN GR|LFP and (b) GR|LFP full-cells.

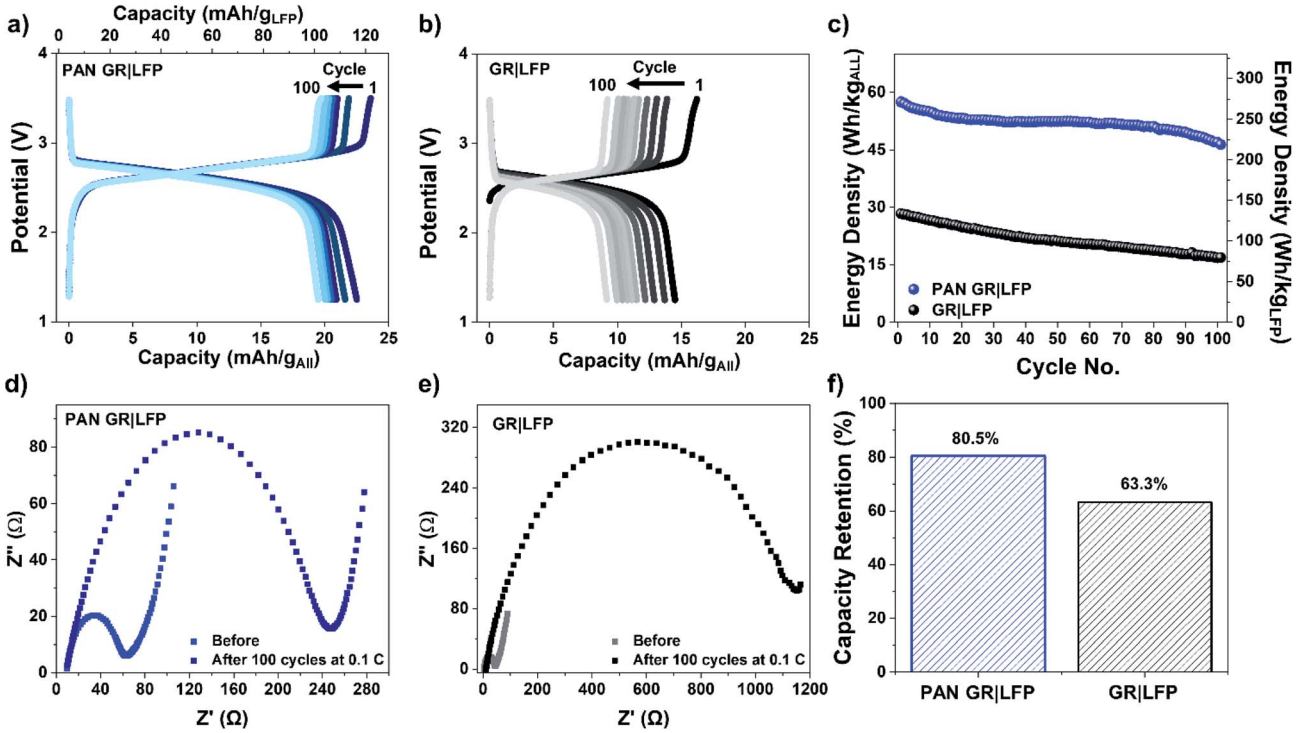

Fig. 4 Charge discharge curves of every 10th cycle of galvanostatic cycling at 0.1 C for (a) PAN GR|LFP and (b) GR|LFP full-cells, (c) energy density *vs.* cycle number with respect to total mass (left *y*-axis) and LFP active material (right *y*-axis), electrochemical impedance spectroscopy spectra of (d) PAN GR|LFP and (e) GR|LFP full-cells before and after 100 cycles at 0.1 C, and (f) capacity retention over 100 cycles at 0.1 C.

anode and cathode lead to a significantly less electroactive surface area for structural batteries without PAN coating. Following this over 100 subsequent cycles at a slow cycling rate of 0.1 C, the PAN GR|LFP electrode retains over 80% of its initial capacity whereas the GR|LFP (without PAN) electrode retains less than 64% of initial capacity after formation cycling (Fig. 4f). Similar trends in performance were observed during half-cell cycling and are included in Fig. S1–S6, ESI.† GR|Li and LFP|Li half-cells with the addition of PAN had improved capacity retention and cycling compared to those without the addition of the PAN polymer layer.

While the objective of battery design is to achieve a high gravimetric energy density relative to the mass of active battery materials, the objective of a structural battery is to further design an integration pathway that can achieve a high gravimetric energy density relative to all battery and composite materials. In this manner, we measured the gravimetric energy density of both inactive (structural) and active (battery) materials in the battery composite, including the carbon fiber. We then measure the average energy density over a period of 100 cycles for PAN GR|LFP electrodes to be 52 W h kg^{-1} (maximum $\sim$ 58 W h kg^{-1}), more than two times greater than the GR|LFP electrodes with an average energy density of 21 W h kg^{-1} (Fig. 4c). This energy density of the PAN GR|LFP structural batteries is about 1/3 that of a packaged Li-ion commercial cell and includes the structural carbon fiber composite materials that serve both as the inactive packaging for this structural battery as well as a component for the structural design of the system. In this regard, we believe that the next-generation design of high-performance batteries will optimize the total system gravimetric performance, as opposed to improvements in cell-level performance without consideration of the system the battery is plugged into.

Furthermore, electrochemical impedance spectroscopy (EIS) was also performed to probe the kinetics of the electrode process and interface properties with and without PAN before and after cycling. PAN containing electrodes are often used as a polymer binder due to low charge transfer resistance R_{CT} associated with polar nitrile groups.[58] EIS measurements (Fig. 4d and e) indicate an initial R_{CT} of 60 Ω with PAN and of 45 Ω without PAN. However, after cycling with no PAN R_{CT} ($R_{CT} \sim$ 1140 Ω) (Fig. 4e) was 80% greater than with the addition of PAN ($R_{CT} \sim$ 240 Ω) (Fig. 4d) further proving that the loss of interface integrity without PAN stabilization that leads to poorer cycling stability of the structural battery. While the initial impedance of the full-cell with PAN is slightly higher than that without PAN, we attribute this to the PAN layer reducing cell conductivity. However, after cycling the small increase in resistance due to the PAN layer is overshadowed by the positive effect that PAN has on the stability of the electrode material interface, resulting in a significantly larger R_{CT} for the case without PAN. Notably, such an increase in R_{CT} after cycling is commonly attributed to cell aging and material delamination in Li-ion battery systems,[59] consistent with our other results for structural batteries prepared without PAN. Thereby, this further elucidates that PAN improves the interphase between the fibers and the matrix

which minimizes material delamination, resulting in a lower R_{CT} after cycling and enhanced electrochemical performance.

Additionally, to evaluate the role of the PAN coating on the rate capability of the structural batteries, we tested six cycles at rates of 0.1 C, 0.2 C, 0.5 C, 0.7 C, and 1 C, as shown in Fig. S10, ESI.† Overall, at 1 C the PAN based batteries maintain ~ 68% of the 0.1 C capacity whereas the structural batteries without PAN maintain ~ 60%. However, these results indicate consistent trends of less capacity retention in structural batteries prepared with PAN coatings, which is also evident in Fig. 4c.

Further, when evaluating a multifunctional device, it is important to quantify the benefit or advantage of the design approach and performance relative to the individual (separate) devices that are being combined. From a broad perspective, the approach we demonstrate effectively utilizes the composite materials including carbon fiber and epoxy matrix as packaging (inactive) materials for the battery – even though these components are associated with the gravimetric footprint of the system as well. In turn, even the structural materials (*e.g.* carbon fiber, epoxy, *etc.*) play an active role in the multifunctional device for structural performance, making no portion of this structural battery design inactive under structural and multifunctional operation. Our findings of this work indicate that the active battery materials are more effectively utilized in the PAN-coated composite *versus* the non-PAN coated one. Therefore, to quantitatively evaluate and compare the multifunctional advantage in this structural battery with PAN coatings, we adopted the formalism introduced by Sun *et al.*[22] to evaluate the multifunctional advantage of structural rGO-polymer supercapacitors. Detailed calculations for the multifunctional advantage are presented in Fig. S16, ESI.† Overall, we calculated the multifunctional advantage for the PAN-coated structural battery to be 1.08 *versus* 0.78 for the uncoated structural battery, which is attributed to the ~2× larger total gravimetric energy density of this device. Following this formalism, an overall multifunctional advantage >1 indicates potential for significant system-level volume or cost savings of the multifunctional material compared to individual battery and structural material components. In other words, the performance of the system plus the battery using a multifunctional integration scheme is improved in comparison to the traditional pathway of incorporating the separate (single function) elements together. Therefore, this highlights a significant point that even with a structural battery design that eliminates inactive materials, the lack of appropriate interface reinforcement – especially in the case of volume-changing battery materials, can lead active materials to become inactive during operation. In turn, our work not only highlights the first structural lithium ion battery with a demonstrated multifunctional advantage >1, but also highlights the significant science of interface design that must be addressed in ongoing efforts in this field to achieve practical device outcomes.

Conclusion

In summary, our findings demonstrate the importance of a PAN interface that bridges the active battery materials and epoxy matrix in a structural lithium ion battery to enable (1) reinforced mechanical adherence between the active battery materials and carbon fiber current collector, and (2) active ion transport pathways between the composite matrix and active materials *via* the PAN. This enables us to achieve average energy density measured over 100 cycles in a structural lithium-ion battery, considering both active battery materials and composite materials, to be ~52 W h kg^{-1}, with a maximum energy density of ~58 W h kg^{-1}. Compared to traditional commercially packaged LIBs, which incorporate inactive packaging and bear no on-board mass of system components in gravimetric energy density (*e.g.* carbon fibers, epoxy, *etc.*), the calculated multifunctional advantage >1 in our work enables the structural battery to yield improved system level performance over separately combined LIBs and composite structural materials, a key milestone for structural energy storage. Overall, this performance is ~2× improved for structural batteries without PAN and we attribute the lower energy density in the uncoated structural battery to the delamination of active materials during both SEI formation cycles and subsequent charge–discharge cycling of the full-cell structural battery.

Overall, this work shows that engineering stable interfaces, in our case with PAN, is an important ongoing step toward achieving structural batteries with a clearly defined multifunctional advantage over separate components in a system. In turn, we demonstrate the first structural battery with a clearly defined advantage compared to a separate carbon fiber structural composite and Li-ion battery. With the broad societal relevance of batteries in systems where the total system gravimetric footprint (structural materials + batteries) is evaluated together – such as in aerospace systems, electric vehicles and transportation, electric powered maritime applications, electric powered appliances and power tools, and other emerging mobile devices, improving the total energy stored on board while decreasing the weight of the system using multifunctional batteries can be viewed as analogous to the conventional path of achieving higher energy density batteries that can externally be added in a modular fashion to a system with the same gravimetric footprint. Our work shows for the first time that the prospect for battery integration into structural materials in a way that provides improved system performance or cost is a realizable future goal.

Experimental section

Electrode fabrication and battery assembly

Carbon fiber (Fibre Glast) was used as the current collector for all electrodes. Lithium iron phosphate (LFP) electrodes consisted of LFP (MTI), conductive carbon black (MTI), multiwall carbon nanotubes (CheapTubes, >95%), and PVDF binder (MTI, >99.5%) in a ratio of 65 : 20 : 5:10, respectively. Carbon nanotubes were used as a conductive additive to offset the insulating nature of the carbon fiber current collector and increase the conductivity throughout the cathode.[60] Graphite (GR) electrodes were made with graphite powder <20 μm (Sigma-Aldrich), conductive carbon black (MTI), and PVDF binder (MTI, >99.5%) in a ratio of 80 : 10 : 10, respectively. Full-cells were assembled with a N/P ratio of 2.1 : 1.

A polyacrylonitrile (PAN) coating was made by dissolving 2.5 wt% PAN in dimethylformamide (Sigma-Aldrich, 99.8%) and stirring at 70 °C.[61] PAN GR and PAN LFP electrodes were made by coating the GR and LFP electrodes, respectively, with PAN. Celgard 2525 separators were used with 1 M $LiPF_6$ (Sigma-Aldrich, 98%) in ethylene carbonate (Sigma-Aldrich, 98%) : diethyl carbonate (Sigma-Aldrich, 99%) in a 1 : 1 volume ratio as the electrolyte. Carbonate solvents were chosen as a control to minimize water contamination issues more heavily associated with other solvents like ionic liquids. Galvanostatic testing was performed on an 8 channel MTI battery testing system and cyclic voltammetry and electrochemical impedance spectroscopy (EIS) were conducted using a Metrohm Autolab potentiostat/galvanostat. EIS was performed at room temperature (25 °C) from 1 000 000 Hz – 0.1 Hz for 100 frequencies, a single sine wave logarithmic frequency step with amplitude 0.05 V with a SOC before and after cycling ~100% after resting for 24 hours so that the voltage was stable.

Carbon fiber composite battery assembly

The carbon fiber layup process used epoxy (Fibre Glast Developments Corp., System 1000 Laminating Epoxy Resin Standard Part Kit 1000/1025), a roller, squeegee, and carbon fiber (Fibre Glast). 4 pieces of 6 cm × 6 cm carbon fiber were impregnated with epoxy. The composite battery was then assembled similarly too;[39] two of the epoxy-impregnated carbon fiber squares, GR|CF electrodes with and without PAN, a separator, a LFP|PAN electrode with and without PAN, and two-epoxy impregnated carbon fiber squares. Nickel tabs (MTI, 99.99%) were used for the GR|LFP electrode and aluminum tabs (MTI, 99.99%) were used for the LFP|PAN electrode.

Electrode characterization and mechanical testing

All electrode materials were examined by scanning electron microscopy using a Zeiss Merlin SEM. An Instron mechanical tester was used to perform lap shear tensile tests and carbon fiber composite tensile tests. All samples underwent tensile tests at a strain rate of 2 mm min^{-1}.

Conflicts of interest

There are no conflicts to declare.

Acknowledgements

The authors thank Alex Stephens, Jacob Fine, Elyssa Ferguson, and Ezra Brody for helpful discussions and Robin Midgett for use of the Instron mechanical tester. K. M. and J. E. R. were supported by NSF 1445197.

References

1 M. Li, J. Lu, Z. Chen and K. Amine, *Adv. Mater.*, 2018, **30**, 1800561.
2 S. V. Kalinin, O. Dyck, N. Balke, S. Neumayer, W.-Y. Tsai, R. Vasudevan, D. Lingerfelt, M. Ahmadi, M. Ziatdinov, M. T. McDowell and E. Strelcov, *ACS Nano*, 2019, **13**, 9735–9780.
3 R. Schmuch, R. Wagner, G. Hörpel, T. Placke and M. Winter, *Nat. Energy*, 2018, **3**, 267–278.
4 A. Sakti, J. J. Michalek, E. R. H. Fuchs and J. F. Whitacre, *J. Power Sources*, 2015, **273**, 966–980.
5 A. Manthiram, X. Yu and S. Wang, *Nat. Rev. Mater.*, 2017, **2**, 16103.
6 L. H. Saw, Y. Ye and A. A. O. Tay, *J. Cleaner Prod.*, 2016, **113**, 1032–1045.
7 A. Kwade, W. Haselrieder, R. Leithoff, A. Modlinger, F. Dietrich and K. Droeder, *Nat. Energy*, 2018, **3**, 290–300.
8 A. Magasinski, P. Dixon, B. Hertzberg, A. Kvit, J. Ayala and G. Yushin, *Nat. Mater.*, 2010, **9**, 353–358.
9 Y. Jin, B. Zhu, Z. Lu, N. Liu and J. Zhu, *Adv. Energy Mater.*, 2017, **7**, 1700715.
10 M. T. M. Y. Cui, in *Semiconductor Nanowires: from Next-Generation Electronics to Sustainable Energy*, ed. J. X. W. Lu, Royal Society of Chemistry, 2014, ch. 8.
11 C. K. Chan, H. Peng, G. Liu, K. McIlwrath, X. F. Zhang, R. A. Huggins and Y. Cui, *Nat. Nanotechnol.*, 2008, **3**, 31–35.
12 Y.-K. Sun, D.-J. Lee, Y. J. Lee, Z. Chen and S.-T. Myung, *ACS Appl. Mater. Interfaces*, 2013, **5**, 11434–11440.
13 X. Ding, X. Huang, J. Jin, H. Ming, L. Wang and J. Ming, *J. Power Sources*, 2018, **379**, 53–59.
14 A. S. Westover, J. W. Tian, S. Bernath, L. Oakes, R. Edwards, F. N. Shabab, S. Chatterjee, A. V. Anilkumar and C. L. Pint, *Nano Lett.*, 2014, **14**, 3197–3202.
15 A. S. Westover, B. Baer, B. H. Bello, H. Sun, L. Oakes, L. M. Bellan and C. L. Pint, *J. Mater. Chem. A*, 2015, **3**, 20097–20102.
16 J. Tao, N. Liu, W. Ma, L. Ding, L. Li, J. Su and Y. Gao, *Sci. Rep.*, 2013, **3**, 2286.
17 N. Muralidharan, E. Teblum, A. S. Westover, D. Schauben, A. Itzhak, M. Muallem, G. D. Nessim and C. L. Pint, *Sci. Rep.*, 2018, **8**, 17662.
18 Z. Jiao, Q. Wu, L. Cardon and J. Qiu, *J. Nanosci. Nanotechnol.*, 2020, **20**, 2316–2323.
19 P. Flouda, S. A. Shah, D. C. Lagoudas, M. J. Green and J. L. Lutkenhaus, *Matter*, 2019, **1**, 1532–1546.
20 P. Flouda, X. Feng, J. G. Boyd, E. L. Thomas, D. C. Lagoudas and J. L. Lutkenhaus, *Batteries Supercaps*, 2019, **2**, 464–472.
21 B. K. Deka, A. Hazarika, J. Kim, Y.-B. Park and H. W. Park, *Int. J. Energy Res.*, 2017, **41**, 1397–1411.
22 W. Sun, S. A. Shah, J. L. Lowery, J. H. Oh, J. L. Lutkenhaus and M. J. Green, *Adv. Mater. Interfaces*, 2019, **6**, 1900786.
23 N. Liu, Z. Lu, J. Zhao, M. T. McDowell, H.-W. Lee, W. Zhao and Y. Cui, *Nat. Nanotechnol.*, 2014, **9**, 187.
24 T. Pereira, Z. Guo, S. Nieh, J. Arias and H. T. Hahn, *J. Compos. Mater.*, 2009, **43**, 549–560.
25 T. Pereira, Z. Guo, S. Nieh, J. Arias and H. T. Hahn, *Compos. Sci. Technol.*, 2008, **68**, 1935–1941.
26 P. Ladpli, R. Nardari, F. Kopsaftopoulos and F.-K. Chang, *J. Power Sources*, 2019, **414**, 517–529.

27 H. Cheng, Z. Liu, H. Huang, X. Sun and Z. Li, *Polym. Compos.*, 2015, **36**, 961–968.
28 J. F. Snyder, E. L. Wong and C. W. Hubbard, *J. Electrochem. Soc.*, 2009, **156**, A215–A224.
29 W. Johannisson, D. Zenkert and G. Lindbergh, *Multifunctional Materials*, 2019, **2**, 035002.
30 W. Johannisson, N. Ihrner, D. Zenkert, M. Johansson, D. Carlstedt, L. E. Asp and F. Sieland, *Compos. Sci. Technol.*, 2018, **168**, 81–87.
31 A. Javaid and M. Z. Ali, *Mater. Res. Express*, 2018, **5**, 055701.
32 E. Jacques, M. H. Kjell, D. Zenkert and G. Lindbergh, *Carbon*, 2014, **68**, 725–733.
33 N. Ihrner, W. Johannisson, F. Sieland, D. Zenkert and M. Johansson, *J. Mater. Chem. A*, 2017, **5**, 25652–25659.
34 Q. Han, W. Zhang, Z. Han, S. Niu, J. Zhang, F. Wang, X. Li, D. Geng and G. Yu, *Ionics*, 2019, **25**, 5333–5340.
35 G. Fredi, S. Jeschke, A. Boulaoued, J. Wallenstein, M. Rashidi, F. Liu, R. Harnden, D. Zenkert, J. Hagberg, G. Lindbergh, P. Johansson, L. Stievano and L. E. Asp, *Multifunctional Materials*, 2018, **1**, 015003.
36 F. Dionisi, R. Harnden and D. Zenkert, *Compos. Struct.*, 2017, **179**, 580–589.
37 D. Carlstedt and L. E. Asp, *Compos. Sci. Technol.*, 2019, **179**, 69–78.
38 K. Moyer, C. Meng, B. Marshall, O. Assal, J. Eaves, D. Perez, R. Karkkainen, L. Roberson and C. L. Pint, *Energy Storage Mater.*, 2020, **24**, 676–681.
39 K. Share, A. Westover, M. Li and C. L. Pint, *Chem. Eng. Sci.*, 2016, **154**, 3–19.
40 J. Moon, J. Y. Jeong, J. I. Kim, S. Kim and J. H. Park, *J. Power Sources*, 2019, **416**, 89–94.
41 E. Kazyak, K. N. Wood and N. P. Dasgupta, *Chem. Mater.*, 2015, **27**, 6457–6462.
42 E. Kazyak, K.-H. Chen, K. N. Wood, A. L. Davis, T. Thompson, A. R. Bielinski, A. J. Sanchez, X. Wang, C. Wang, J. Sakamoto and N. P. Dasgupta, *Chem. Mater.*, 2017, **29**, 3785–3792.
43 N. P. Dasgupta, H. J. Jung, O. Trejo, M. T. McDowell, A. Hryciw, M. Brongersma, R. Sinclair and F. B. Prinz, *Nano Lett.*, 2011, **11**, 934–940.
44 Y. Chen, N. J. Ginga, W. S. LePage, E. Kazyak, A. J. Gayle, J. Wang, R. E. Rodríguez, M. D. Thouless and N. P. Dasgupta, *ACS Appl. Mater. Interfaces*, 2019, **11**, 43573–43580.
45 Y. Zhang, Y.-Z. Song, J.-J. Yuan, X. Yin, C.-C. Sun and B.-K. Zhu, *J. Appl. Polym. Sci.*, 2018, **135**, 46423.
46 J. Yun, I. Echols, P. Flouda, S. Wang, A. Easley, X. Zhao, Z. Tan, E. Prehn, G. Zi, M. Radovic, M. J. Green and J. L. Lutkenhaus, *ACS Appl. Mater. Interfaces*, 2019, **11**, 47929–47938.
47 J. Luo, C.-C. Fang and N.-L. Wu, *Adv. Energy Mater.*, 2018, **8**, 1701482.
48 J. Lopez, D. G. Mackanic, Y. Cui and Z. Bao, *Nat. Rev. Mater.*, 2019, **4**, 312–330.
49 Y. Kwon, Y. Lee, S.-O. Kim, H.-S. Kim, K. J. Kim, D. Byun and W. Choi, *ACS Appl. Mater. Interfaces*, 2018, **10**, 29457–29466.
50 B. H. Shen, S. Wang and W. E. Tenhaeff, *Sci. Adv.*, 2019, **5**, eaaw4856.
51 J. O. K. Surendra, K. Martha, J. Nanda and N. J. Dudney, *J. Electrochem. Soc.*, 2011, **158**, A1060–A1066.
52 S. K. Kumar, S. Ghosh, S. K. Malladi, J. Nanda and S. K. Martha, *ACS Omega*, 2018, **3**, 9598–9606.
53 J. Zhu, Y. Wu, X. Huang, L. Huang, M. Cao, G. Song, X. Guo, X. Sui, R. Ren and J. Chen, *Nano Energy*, 2019, **62**, 883–889.
54 W. Zhang, Y. Weng, W. Shen, R. Lv, F. Kang and Z.-H. Huang, *Carbon*, 2020, **158**, 163–171.
55 G. Shoorideh, B. Ko, A. Berry, M. J. Divvela, Y. S. Kim, Z. Li, B. Patel, S. Chakrapani and Y. L. Joo, *ACS Appl. Energy Mater.*, 2018, **1**, 1106–1115.
56 J. Xu and J. Varna, *J. Compos. Mater.*, 2019, **53**, 3615–3628.
57 N. Elgrishi, K. J. Rountree, B. D. McCarthy, E. S. Rountree, T. T. Eisenhart and J. L. Dempsey, *J. Chem. Educ.*, 2018, **95**, 197–206.
58 L. Gong, M. H. T. Nguyen and E.-S. Oh, *Electrochem. Commun.*, 2013, **29**, 45–47.
59 A. H. Jochen Bernhard Gerschler and D. U. Sauer, *Tech. Mitt.*, 2006, **99**, 214–220.
60 G. Qin, Q. Wu, J. Zhao, Q. Ma and C. Wang, *J. Power Sources*, 2014, **248**, 588–595.
61 C. Pirlot, Z. Mekhalif, A. Fonseca, J. B. Nagy, G. Demortier and J. Delhalle, *Chem. Phys. Lett.*, 2003, **372**, 595–602.

